CHAPTER 7

Co-pyrolysis of low rank coal and de-oiled microalgae biomass for bio-oil production using synthesized catalyst[*]

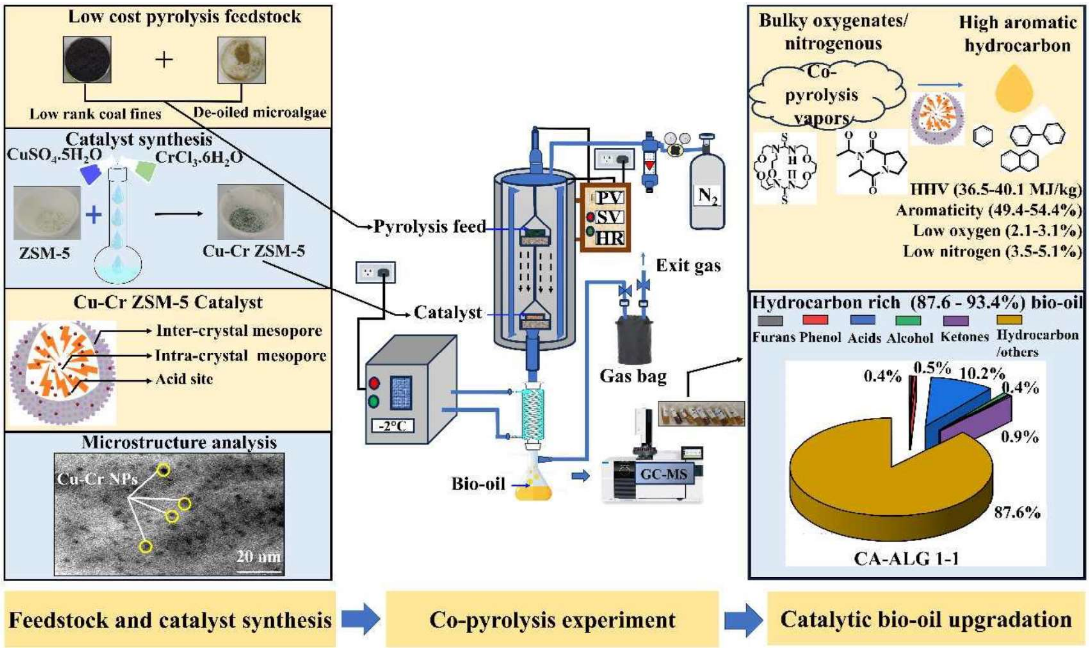

---

[*] This work is published in **Shweta Rawat, Alok Kumar Singh, Jyoti Prasad Chakraborty, Sanjay Kumar (2024b)** Characterization and mechanism elucidation of high-quality bio-oil production from co-pyrolysis of waste low-rank coal fines and de-oiled microalgae biomass using bimetallic (Cu-Cr) ZSM-5 catalyst. Journal of Environmental Chemical Engineering. 113046.

Abstract

The present chapter provides a cleaner co-pyrolysis strategy for high-quality bio-oil production by utilizing low-cost residues such as low-rank coal (CL), de-oiled microalgae (ALG), and their blends (CLALG). The heavy metal-loaded Cu-Cr-ZSM-5 catalyst is synthesized by using ion-exchange method and investigated in the CL, ALG and CLALG pyrolysis bio-oil upgradation at different catalyst feed ratios (0.5:1, 1:1, 2:1). The synthesized catalyst is characterized by x-ray diffraction (XRD), scanning electron microscopy (SEM), transmission electron microscopy (TEM) and brunauer-emmett-teller (BET) analysis. The synthesized catalyst is nano-crystalline of average size 7 nm. The microstructure of the synthesized catalyst shows stacked nanorods packing with connected intercrystal and intracrystal mesopores. The catalytic and non-catalytic pyrolysis of CL, ALG and CLALG are performed at 600 °C, 10 °C/min for 60 min. The non-catalytic ALG pyrolysis has shown maximum bio-oil yield (35.7 %). The synergistic effect of nanorod morphology, active acid sites and excess mesoporosity of catalyst facilitates efficient deoxygenation, denitrogenation and aromatization of pyrolysis bio-oil with oxygen content from 2.1–3.1 %, nitrogen content 3.5–5.1 % and aromatic content 49.4–54.4 % at catalyst feed ratio of 1:1. The maximum obtained higher heating value (HHV) of bio-oil from catalytic pyrolysis of CL (40.1 MJ/kg) followed by CLALG (38.6 MJ/kg) and ALG (36.5 MJ/kg) is very close to diesel oil with HHV (42–46 MJ/kg). Further, a co-pyrolysis mechanism is proposed to systematically investigate possible catalytic action sites to yield high-quality bio-oil. Thus, the outcomes of the present chapter enrich information regarding catalyst development, catalyst feed interaction, and thermocatalytic cracking as emerging efforts towards industrial-scale upgradation of bio-oil to engine fuels.

7.1 Background

The present chapter provides a cleaner co-pyrolysis strategy for high-quality bio-oil production by utilizing low-cost residues such as low rank coal (CL), de-oiled microalgae (ALG) and their blends (CLALG). In the direction of energy transition from fossil fuels to bioenergy, pyrolysis has emerged as a cost-efficient and scalable technology that can convert potential feedstocks such as microalgae (Qiu et al., 2023), low-density and high-density polyethylene (Abnisa et al., 2021), sewage sludge (Wu et al., 2024) and low rank coal to bio-oil (Rawat and Kumar, 2023b).

Based on synergistic interaction studies, de-oiled microalgae (ALG) and low-rank coal (CL) pyrolysis may be considered as an alternative strategy for maximum energy recovery with waste minimization (Khan et al., 2022). However, low rank coal pyrolysis yields bio-oil dominated by tar, which cannot be used as direct fuel (Sardi et al., 2022). By-product, coal tar is a highly viscous black or dark brown product (Sardi et al., 2022). During conventional or non-catalytic pyrolysis, tar adversely affects bio-oil yield and reduces HHV (Sardi et al., 2022).

Similarly, key limitations associated with bio-oil derived from non-catalytic microalgae pyrolysis include high oxygen content, high nitrogen content and high acid content, which results low HHV, high viscosity and more CO_2 emission during oil combustion (Tang et al., 2021). The co-pyrolysis of CL containing low to medium sulfur content (0.5–5 %) and ALG with average S content (< 1.5 %) results bio-oil with S contamination (Chou et al., 2012; Arif et al., 2021). However, high HHV with low N/C, O/C, and S/C ratios are desired for better emission control during oil combustion (Tang et al., 2021). In this direction, pyrolysis of CL, ALG, and their blends (CLALG) produce bio-oil with low energy content and undesired properties, which must be improvised to match transportation fuel standards.

To overcome the challenges of non-catalytic pyrolysis, the catalytic pyrolysis process is a promising approach to upgrade bio-oil quality at low-pressure requirements (Cheah et al., 2023). Among different catalysts, zeolite has been considered the most efficient catalyst with the shape-selective effect of mesoporous-microporous structure (Wu et al., 2024). Towards catalytic activity enhancement, researchers have modified the zeolite structure by incorporating metals such as Cu (Kumar et al., 2017), Cr (Chiosso et al., 2023), Ni (Zainan et al., 2018), Fe (Yashnik et al., 2022), Mo (Mustapha et al., 2021), Ga (Bi et al., 2020) and Mg (Mo et al., 2020). After metal assimilation, new catalytic active sites improve catalytic cracking inside the pores of the catalyst to upgrade bio-oil quality. Different transition metals show specific catalytic actions during hydrocarbon cracking, such as Ni/Mo ZSM-5, responsible for polycyclic compound ring opening (Zainan et al., 2018; Mustapha et al., 2021). The 2–5 % (w/w) metal loading of Cr/Fe ZSM-5 effectively converts aliphatic hydrocarbons to monoaromatic hydrocarbons such as toluene, xylene, and benzene (Chiosso et al., 2023). Although excessive metal loading of 10 % (w/w) deteriorates the physical characteristics of the catalyst, it negatively impacts reactant and product diffusion (Chiosso et al., 2023).

Cu/Fe/Cr metals are better options for low-cost catalyst development than Ni/Co/Mo/Ga due to easy availability, stability, and cost-effectiveness (Chiosso et al., 2023; Mo et al., 2020). Metal-loaded ZSM-5 provides better catalytic active sites formation, enhanced porosity and rapid diffusivity across mesopores/micropores, which causes cracking of bulky oxygenated compounds with improved aromatic production than conventional ZSM-5 (Iliopoulou et al., 2012). Recently, ZSM-5 is successfully applied for catalytic pyrolysis of different potential feedstocks such as microalgae, i.e. *Nannochloropsis* sp. (Zhang et al., 2022), *S. obliquus* (Mustapha et al., 2021), *S. platensis*

(Tang et al., 2021), wood (Kim et al., 2019), coal (Sardi et al., 2022), municipal solid waste (Li et al., 2020) and plastic waste (Khazaal et al., 2023).

Based on an extensive literature review of bio-oil production from non-catalytic and catalytic pyrolysis, the present chapter covers novel bimetallic Cu and Cr incorporated ZSM-5 catalyst synthesis and characterization. Further, product composition analysis of bio-oil from non-catalytic and catalytic pyrolysis are explained. In next stage, the quality of bio-oil from non-catalytic and catalytic pyrolysis are compared.

At end, the chapter proposes a possible reaction mechanism to explore catalyst interaction with primary volatiles during pyrolysis. In-depth analysis of catalytic pyrolysis provides the impact of bimetallic Cu-Cr-ZSM-5 catalyst on bio-oil quality with aspects of thermal stability and textural properties such as meso-microporosity, acid sites, and porosity distribution. The outcomes of present study may be considered a basic framework for cleaner bio-oil production through catalytic pyrolysis to ensure energy security with reduced environmental impact.

7.2 Materials and methods

7.2.1 Materials

The CL and ALG were utilized as co-pyrolysis feedstock to conduct catalytic co-pyrolysis studies. CL was obtained from Singrauli coalfield, India (longitude 82026′11.86″ E, latitude 2405′2.56″ N). The essential preprocessing steps – screening, pulverization, sieving, and drying were performed to obtain coal fines with particle size < 0.25 mm as described in section 5.2.1. The freshwater microalgae *C. pyrenoidosa* NCIM 2738 was utilized as a pyrolysis co-material with CL. Microalgae cultivation, harvesting, de-oiling, sieving and drying were conducted as mentioned in section 3.2.3. Sieved dried algae of particle size < 0.60 mm were mixed with CL at a blending ratio of 57.7 % CL and 42.3 % ALG to form CLALG (ANN-MOGA optimized blending ratio described in the previous section 6.3.7). The proximate and ultimate analysis data of pyrolysis feedstocks CL, ALG and CLALG were estimated according to ASTM D7582-15 standard and ASTM D5373-14 standard, respectively, as described in section 6.2.1. The proximate and ultimate results are summarized in Table 7.1.

Table 7.1 Fuel characteristic analysis of coal (CL), de-oiled microalgae (ALG) and coal and de-oiled microalgae blends (CLALG).

Sample	**Proximate analysis (%)**				**Ultimate analysis (%)**				
	MC	**VM**	**FC**	**A**	**H**	**C**	**N**	**S**	**O**
CL	7.90	13.50	38.60	40.0	4.53	58.86	< 1.00	< 1.00	34.11
ALG	4.94	43.01	34.05	18.0	6.62	45.06	5.67	1.45	41.20
CLALG	6.36	27.11	36.81	29.72	5.41	52.18	3.10	1.19	38.12

Blending ratio of CLALG : 57.7% CL and 42.3% ALG; MC: moisture content; VM: volatile matter; FC: fixed carbon; A: ash content.

7.2.2 Catalyst preparation and characterization

A one-pot synthesis strategy was used for bimetallic Cu and Cr incorporated ZSM-5 zeolite (Cu-Cr-ZSM-5) catalyst preparation via the ion-exchange method. The zeolite ZSM-5 (Si/Al = 23) was purchased from Alfa Aesar, Thermo Fisher Scientific, USA and calcined under an air atmosphere in the furnace at 550 ºC (overnight) to remove impurities before use.

Cu-Cr metal-loaded (5 %) ZSM-5 catalyst was prepared as follows: 20 g of zeolite was mixed with 3.14 g cupric sulfate pentahydrate ($CuSO_4.5H_2O$) and 4.10 g chromium chloride hexahydrate ($CrCl_3.6H_2O$) to make up a solution of 100 ml with distilled water in a beaker as described in reported study (Zainan et al., 2018). The temperature-controlled vigorous stirring of solution was performed at 80 °C for 9 h. Then supernatant was separated from the catalyst mixed solution using vacuum filtration. The remaining filtered residue (Cu-Cr-ZSM-5 catalyst) was dried (100 °C) and then crushed into fine powder. Finally, the synthesized catalyst powder was calcined under an air atmosphere in the furnace at 500 ºC for 5 h, which was further used for characterization and pyrolysis experiments. The schematic representation of Cu-Cr-ZSM-5 catalyst synthesis is shown in Fig. 7.1.

The structural features of synthesized catalysts, such as crystal size and inter-planar spacing between crystallographic planes, were determined using high-resolution powder X-ray diffraction (XRD) (Empyrean, Malvern Panalytical Ltd, Malvern, United Kingdom). The Cu Kα radiation source (λ = 1.5406 nm) was used in the XRD instrument with 30 kV voltage and 30 mA electric current. The diffraction angle (2Θ) was fixed at 10-80º for wide-angle XRD detection. To detect surface morphology of the synthesized Cu-Cr-ZSM-5 catalyst, a field emission scanning electron microscopy (FE-SEM, Quanta 250 FEG series, FEI Co.), with an accelerating voltage of 20 kV, was used.

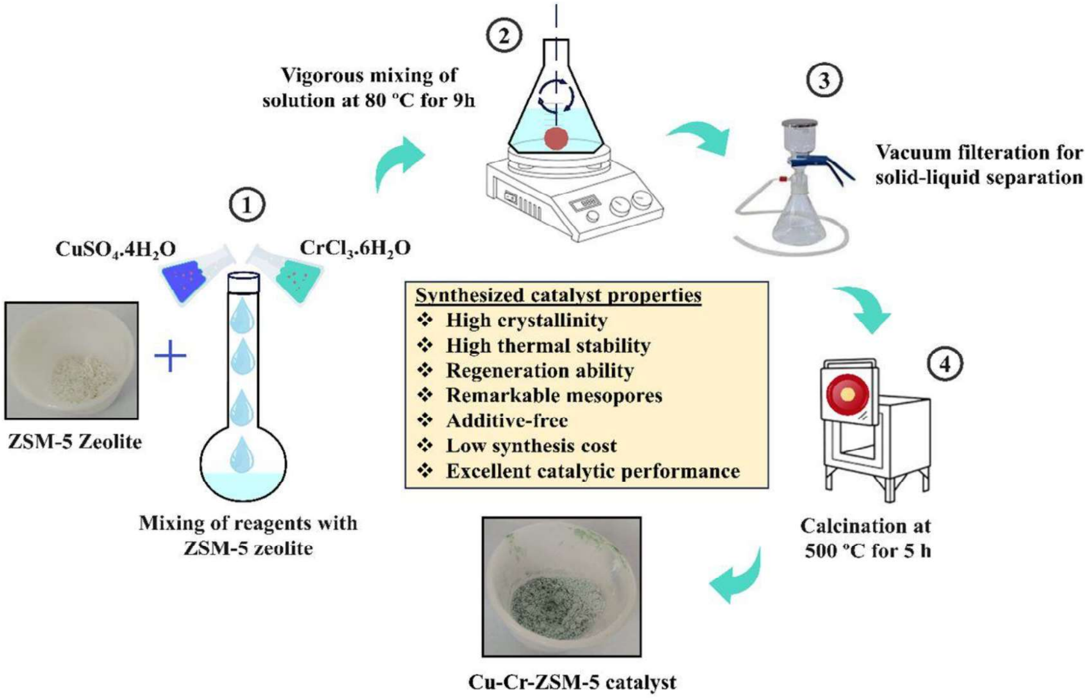

Fig. 7.1 Schematic representation of one-pot synthesis strategy of Cu-Cr-ZSM-5 catalyst.

Further, surface and porosity analyses were performed based on the Brunauer-Emmett-Teller (BET) analysis and t-plot, respectively, while subtracting total pore volume from micropore volume provides mesopore volume. BET analysis was performed on a

Belsorp max instrument (Microtrac BEL instrument, Italy) with 6 h soak time, 200 ºC target temperature and 10 °C/min heating rate. Before the co-pyrolysis experiment, the thermal stability of synthesized Cu-Cr-ZSM-5 and its thermal decomposition compatibility with pyrolysis feedstocks was evaluated via TG–DTG analysis by using TGA-50 thermogravimetric analyzer (Shimadzu, Kyoto, Japan).

7.2.3 Noncatalytic and catalytic pyrolysis of coal and/or de-oiled microalgae

The noncatalytic and catalytic pyrolysis of CL, ALG and CLALG were performed with synthesized Cu-Cr-ZSM-5 catalyst in a two-stage fixed bed tubular reactor as shown in Fig. 7.2.

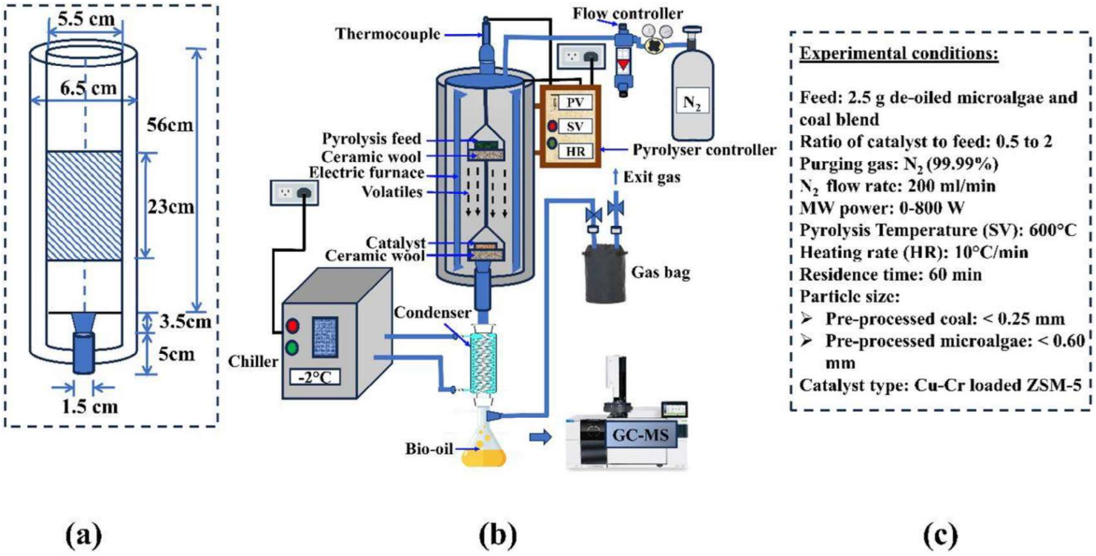

Experimental conditions:

Feed: 2.5 g de-oiled microalgae and coal blend
Ratio of catalyst to feed: 0.5 to 2
Purging gas: N_2 (99.99%)
N_2 flow rate: 200 ml/min
MW power: 0-800 W
Pyrolysis Temperature (SV): 600°C
Heating rate (HR): 10°C/min
Residence time: 60 min
Particle size:
➢ Pre-processed coal: < 0.25 mm
➢ Pre-processed microalgae: < 0.60 mm
Catalyst type: Cu-Cr loaded ZSM-5

Fig. 7.2 Catalytic co-pyrolysis of coal and de-oiled microalgae blend in fixed bed reactor (a) schematic diagram of fixed bed reactor (b) co-pyrolysis set-up (c) experimental conditions of catalytic co-pyrolysis.

The pyrolysis instrument was comprised of feeder, a two-stage fixed bed tubular reactor (56 cm height including 23 cm heating zone and 5.5 cm inner diameter), temperature/ gas flow controller, condensing unit and collection unit. To perform individual as well as catalytic co-pyrolysis experiments, 2.5 g of feedstock material (CL, ALG and

CLALG) was scattered in the quartz wool bed 1 (CW_1) and loaded at the heating zone of the furnace as pyrolysis stage 1. The catalyst was scattered in other quartz wool bed 2 (CW_2) at the bottom of CW_1 as pyrolysis stage 2. The N_2 (99.99 %) was purged from the top of the reactor at a flow rate of 200 ml/min. The pyrolysis experiments were performed at 600 °C, 60 min and 10 °C/min as pyrolysis temperature, residence time and heating rate, respectively. As feedstock material was heated in the first stage, the volatiles flowed through CW_1 and came in direct contact with the catalyst. The catalyst-treated vapors entered the condensing unit connected with the chiller (filled with 40 % isopropanol: 60 % water and set temperature – 2 °C). The condensed bio-oil was stored in a collector.

Further, noncatalytic pyrolysis experiments were conducted under identical operating conditions at single pyrolysis stage 1 by feeding 2.5 g of pyrolysis feedstock (CL, ALG and CLALG) into the furnace without a catalyst. The end products of pyrolysis – biochar and bio-oil were stored for further analysis.

7.2.4 Pyrolysis end-products distribution and energy calculations

The pyrolysis end-products distribution was estimated according to yield Eq. 7.1–7.3 as described in previously reported studies (Li et al., 2020).

$$Y_{Bio-oil} = \frac{m_{Bio-oil}}{m_{Feed}} \times 100\% \tag{7.1}$$

$$Y_{Char} = \frac{m_{Char}}{m_{Feed}} \times 100\% \tag{7.2}$$

$$Y_{Gas} = 100\% - Y_{Bio-oil} - Y_{Char} \tag{7.3}$$

Where, $Y_{Bio\text{-}oil}$, Y_{Char} and Y_{Gas} represented yields of bio-oil, char and gas, respectively. m_{Feed} is referred as mass of CL, ALG or its blend (CLALG). $m_{Bio\text{-}oil}$ and m_{Char} represented as mass of bio-oil and char, respectively.

In pyrolysis experiments, bio-oil production was considered the desired product. Energy yield ($E_{Bio\text{-}oil}$) and energy conversion efficiency ($E_{Conversion\ efficiency}$) was calculated by using Eq. 7.4 and Eq. 7.5.

$$E_{Bio-oil} = Y_{Bio-oil} \times \frac{HHV_{Bio-oil}}{HHV_{Feed}} \tag{7.4}$$

$$E_{Conversion\ efficiency} = \frac{E_{Output}}{E_{Input}} \times 100 \tag{7.5}$$

Where E_{Input} and E_{Output} represented energy input and energy output, respectively and were further calculated by using Eq. 7.6 and Eq. 7.7, respectively.

$$E_{Input} = m_{Feed} \times HHV_{Bio-oil} \tag{7.6}$$

$$E_{Output} = m_{Bio-oil} \times HHV_{Bio-oil} \tag{7.7}$$

7.2.5 Characteristics of noncatalytic and catalytic pyrolysis bio-oil

The physicochemical characterization of bio-oil was performed as the desired end product of pyrolysis. A bomb calorimeter (C 200, IKA, Germany) was utilized for HHV analysis of bio-oil. Bio-oil density was calculated according to the American Society for Testing and Materials (ASTM D1298). A moisture analyzer (Karl Fischer, Esico, India) assessed moisture composition in bio-oil according to ASTM D1744 standard. A digital viscometer (Brookfield DV II Pro) was used to measure bio-oil viscosity. These physicochemical characterizations of bio-oil strongly agreed with previous studies (Bi et al., 2020; Li et al., 2020).

The qualitative chemical information of bio-oil related to functional groups was analyzed by FTIR – Cary 630 FTIR (Agilent, California, USA). Further, different chemical compounds in bio-oil were estimated by Gas chromatography-mass spectrometry (GC-MS) (TQ8040, Shimadzu, Japan) characteristic peaks analysis. Helium was utilized as carrier gas at a 1.5 mL/min flow rate. 1μL of CL, ALG and CLALG oil sample was injected at

300 °C into the column (SH-I-5SIL MS) with dimensions 30 m×0.25mm×0.25μm. The split ratio of the column was 1:20. The start temperature of GC was kept constant at 60 °C for 5 minutes. The maximum final temperature was maintained at 300 °C and a heating rate of 5 °C/min with a hold time of 10 min. The obtained peaks were identified using the National Institute of Standards and Technology library (NIST, USA). The elemental composition of bio-oil obtained from CL, ALG and CLALG pyrolysis was determined through elemental analyzer CHN628 (LECO, Michigan, USA) following ASTM standard D5373-14.

7.3 Results and discussion

7.3.1 Characterization of synthesized Cu-Cr-ZSM-5 catalyst

7.3.1.1 X-ray diffraction

The XRD results of calcined Cu-Cr-ZSM-5 catalyst showed good diffraction intensity and similarity index with parent ZSM-5 catalyst (JCPDS 44-0003) adding minor modification (Fig. 7.3). Considering the standard pdf card (JCPDS 03-0892) of Cu_2O, synthesized catalyst exactly matches with diffraction peak at 2 equal to 36.49 and 42.19, which corresponds to miller indices at 111 and 200. Similarly, the XRD spectra of synthesized catalyst show diffraction peaks at 2ϴ equivalent to 39.7 and 44.22 with corresponding miller indices at 006 and 202, respectively, according to JCPDS 82-1484 of Cr_2O_3.

These results demonstrate successful Cu and Cr species loading on the surface of synthesized catalysts as described in reported studies (Mohanty et al., 2011). The average crystal size of the synthesized catalyst was estimated as 7.00 nm from the XRD pattern Table 7.2). Scherer's equation $D = \frac{k\lambda}{\beta cos\theta}$ was used to calculate the average crystallite size.

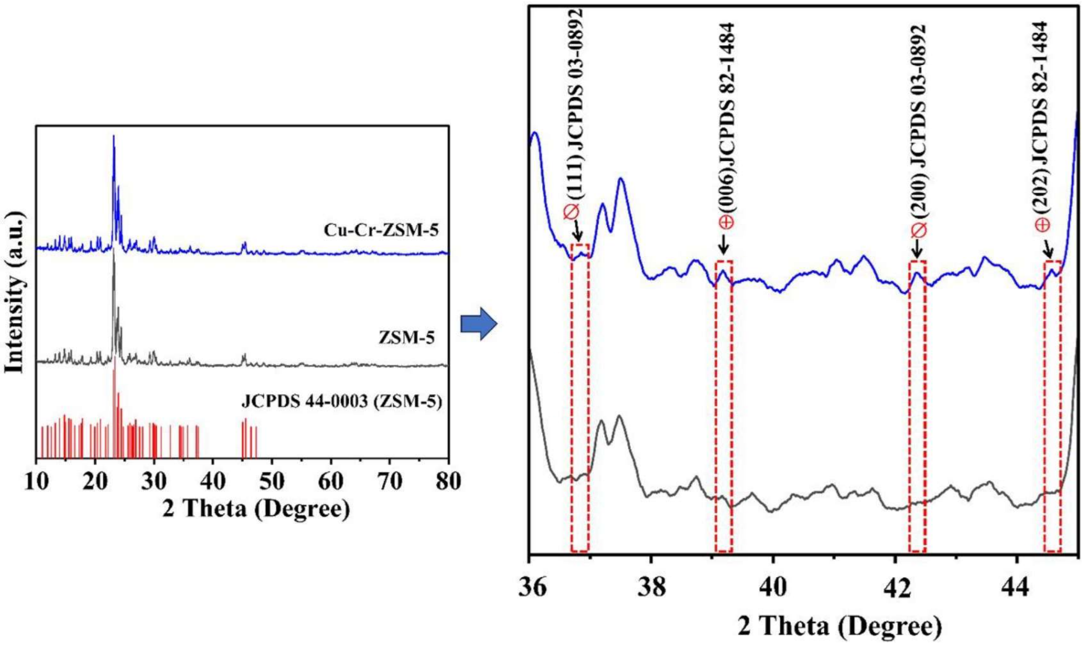

Fig. 7.3 Typical XRD pattern of synthesized Cu-Cr-ZSM-5 and parent ZSM-5 catalyst. (Ø): peak of Cu_2O; (⊕): peak of Cr_2O_3; Parentheses used for Miller Indices (hkl) value corresponding to the respective JCPDS number.

Table 7.2 XRD findings of synthesized Cu-Cr loaded ZSM-5 catalyst.

Peak position 2Θ (degree)	**Peak width FWHM (degree)**	**Inter planer distance (nm)**	**Crystalline size D (nm)**
20.33	1.23	4.37	6.57
23.57	1.23	3.78	6.61
26.69	1.23	3.34	6.65
29.98	1.64	2.98	5.02
41.29	1.02	2.18	8.29
55.22	1.23	1.66	7.30
63.96	1.23	1.46	7.63
70.74	1.23	1.33	7.93
			D_{avg} = 7.00

7.3.1.2 Microstructure characterization

The SEM images of the synthesized Cu-Cr-ZSM-5 catalyst confirm wide particle size distribution (200 nm–10 µm) throughout the sample (Fig. 7.4a – b). The SEM images of the synthesized catalyst demonstrate a defined, dense-packed nanorod structure. It further indicates that nanorods are stacked throughout the particle to formulate microspheres. The aggregated nanorod structure of synthesized Cu-Cr-ZSM-5 catalyst is distinctly different from pure ZSM-5 morphology as reported in existing literature (Lai et al., 2015).

EDS confirms that heavy metals Cu and Cr are incorporated upon the catalyst surface. The elemental mapping, including metal and Si-Al content of heavy metal-loaded catalyst surface, is shown in (Fig. 7.4b). The higher Si/Al ratio is linearly correlated to the strength of active acid sites, represented a highly siliceous zeolite (Miskolczi et al., 2019). Comparing parent ZSM-5 with metal-loaded ZSM-5, it is observed that metal loading decreases the Si/Al ratio, similar to a previous study (Miskolczi et al., 2019). The microstructure of the synthesized catalyst was further characterized in detail by transmission electron microscopy (TEM) at different resolutions (Fig. 7.5).

The high-resolution TEM images showed well-dispersed Cu and Cr nanoparticles on the zeolite surface of the synthesized catalyst (Fig. 7.5a–b). The low-resolution TEM image confirmed the existence of zeolite nanorods and the formation of substantial mesopores due to the stacking of these rods (Fig. 7.5d)). The morphology of synthesized catalyst highly correlates with other reported nanosized ZSM catalyst (Wu et al., 2022). The distinguished lattice fringes in the high-resolution TEM images reflect several adjacent nanorods which are highly oriented parallelly with inter fringe distance of 1.12 nm and assigned lattice plane of [111] as shown in Fig. 7.5c. The selected area electron diffraction patterns suggest that synthesized catalyst is highly crystalline with unidirectional orientation of nanorods (Fig. 7.5e). Similar crystallographic structure with substantial mesopores is reported for synthesized ZSM-5 and ZSM-11 (Shen et al., 2021).

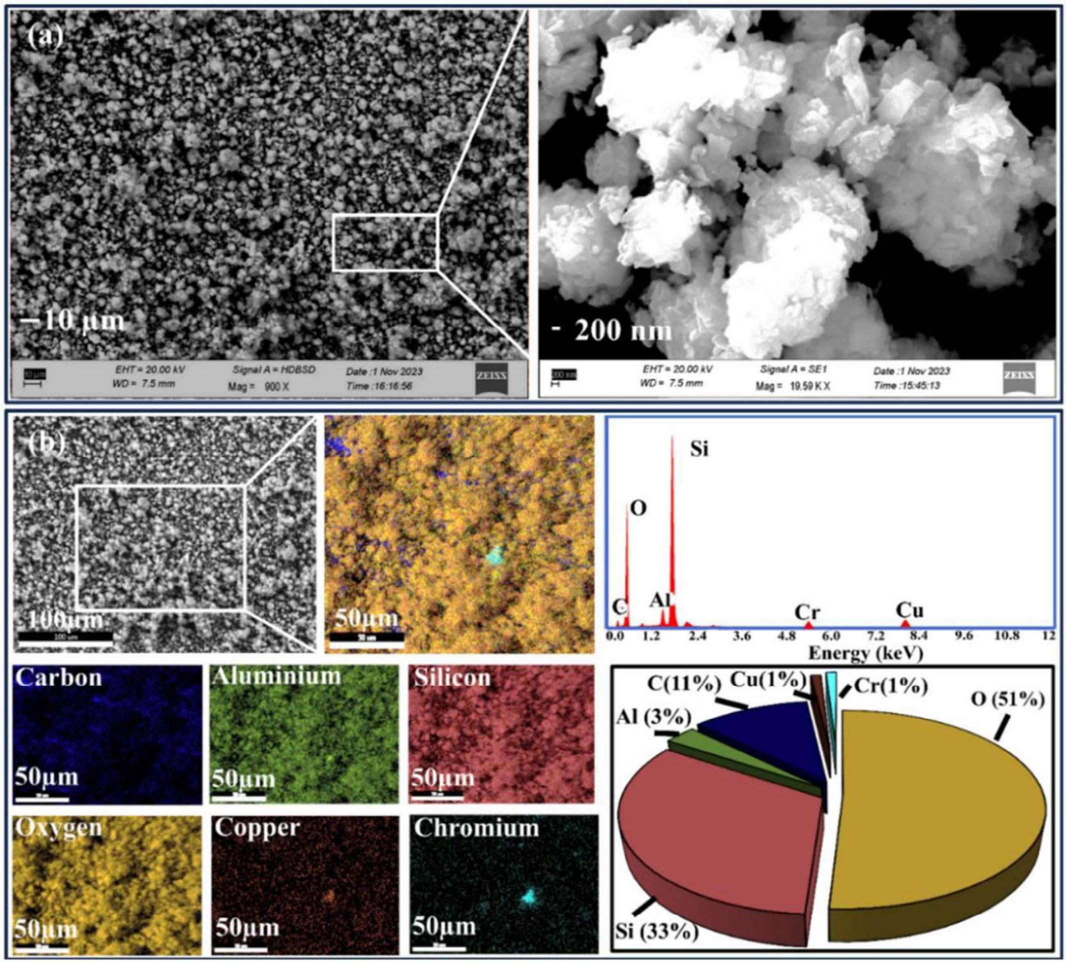

Fig. 7.4 (a) SEM micrograph of synthesized Cu-Cr-ZSM-5 catalyst (b) Elemental mapping of carbon, aluminum, silicon, oxygen, copper, and chromium with weight % distribution in synthesized Cu-Cr-ZSM-5 catalyst.

7.3.1.3 Fourier Transform Infrared analysis

The FTIR spectra for ZSM-5 and Cu-Cr-ZSM-5 confirm that absorption around 1800–500 cm^{-1} is structure sensitive, depending on zeolite types (Fig. 7.6). The asymmetric stretch of Si–O–Al or Si–O–Si in the ZSM-5 framework corresponds to the frequency band at 1099 cm^{-1}. However, a slight shifting in the frequency band (1100 cm^{-1}) is observed for the Cu-Cr-ZSM-5 sample (Fig. 7.6). Asymmetric stretch due to infrared band position at 1221.8 cm^{-1} for the ZSM-5 sample is shifted to 1223 cm^{-1} for Cu-Cr-ZSM-5 sample in agreement with previous studies (Felvey et al., 2020).

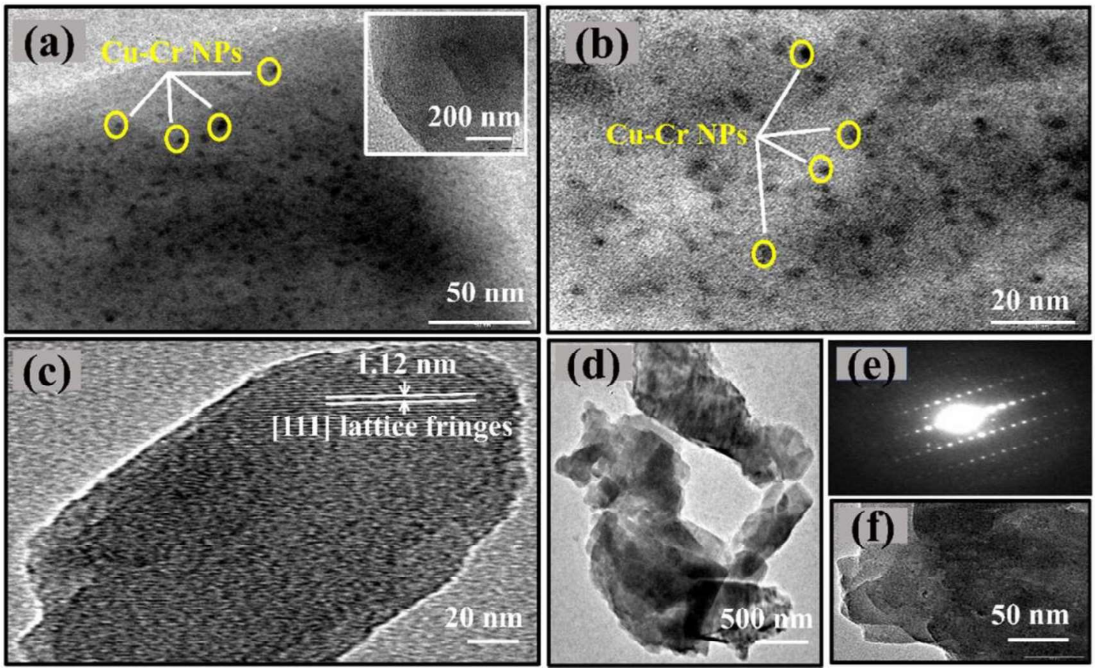

Fig. 7.5 TEM images of (a,b,c,d,f) synthesized Cu-Cr-ZSM-5 catalyst at different resolutions (e) SAED pattern of synthesized Cu-Cr-ZSM-5 catalyst.

The spectral region from 1400–1650 cm^{-1} corresponds to alkenyl (δ CH_2, δ CH_3) and aromatic carbenium ions. In the present IR spectra of ZSM-5, a frequency band at 1607 cm^{-1} is assigned for aromatic carbenium ions, as reported in the previous study (Tabor et al., 2019). The band intensity is further reduced for the Cu-Cr-ZSM-5 catalyst. After calcination of ZSM-5, dispersed Cu and Cr on amorphous SiO_2 indicate that at oxidation state, CuO/ $[Cr(=O)_2]^{2+}$ species is bound to support the surface oxygen of ZSM-5 (Felvey et al., 2020). As reported in the literature, the peak observed at 1767 cm^{-1} is associated with bond formation between Cr and SiO_2 (Felvey et al., 2020). The release of Cu^{2+} ions from $CuSO_4$ for incorporation in ZSM-5 is confirmed by S=O stretching assigned by a peak at 1365 cm^{-1} in Cu-Cr-ZSM-5 spectra. Before and after pyrolysis, FTIR spectra of the Cu-Cr-ZSM-5 catalyst are observed to be identical without any significant changes (Fig. 7.6). It implies that the intrinsic properties of the catalyst are preserved during pyrolysis (Fig. 7.6).

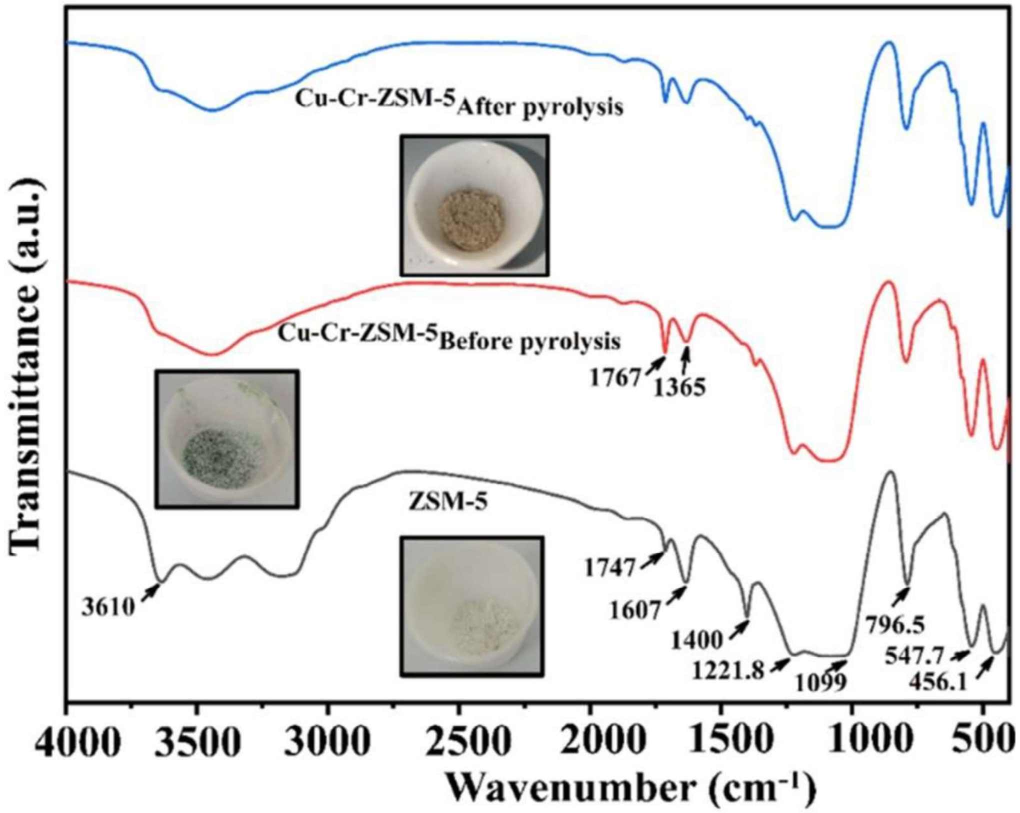

Fig. 7.6 FTIR spectra of parent ZSM-5 catalyst and synthesized Cu-Cr-ZSM-5 catalyst at different pyrolysis stages.

7.3.1.4 Brunauer-Emmett-Teller (BET) surface area analysis

The textural characteristics of Cu-Cr-ZSM-5 catalyst including N_2 adsorption-desorption isotherms, pore size distribution and mesopore-micropore surface analysis is summarized in Fig. 7.7. Interestingly, Cu-Cr-ZSM-5 exhibited combined Type-I and Type-IV isotherms with hysteresis loop (Fig. 7.7). At low-pressure zone ($P/P_0 < 0.001$), the adsorption isotherms showed steeply increased N_2 uptake indicating type I isotherm and microporosity (< 2 nm). At relative pressure, $P/P_0 > 0.8$, absorbed nitrogen is steeply increased and exhibited type IV isotherm with mesoporosity of 2–50 nm. Very few macropores (50–200 nm) are available in the sample. The reported literature on zeolite material also confirms the presence of majorly cylindrical-type mesopores with very few micropores in synthesized Cu-Cr-ZSM-5 (Wu et al., 2024).

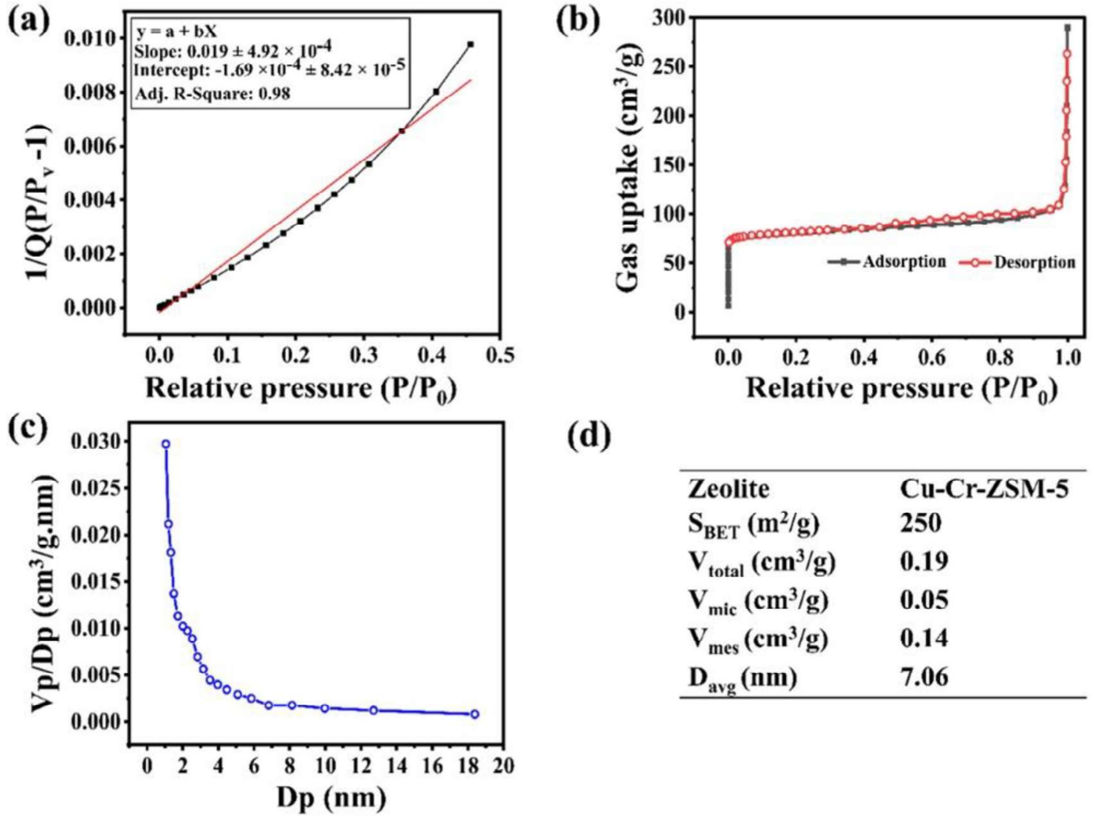

Zeolite	Cu-Cr-ZSM-5
S_{BET} (m^2/g)	250
V_{total} (cm^3/g)	0.19
V_{mic} (cm^3/g)	0.05
V_{mes} (cm^3/g)	0.14
D_{avg} (nm)	7.06

Fig. 7.7 (a) BET surface area analysis. (b) N_2 adsorption-desorption isotherms. (c) pore size distribution (d) textural characteristics of synthesized Cu-Cr-ZSM-5 catalyst. S_{BET}: Specific surface area (m^2/g); V_{total} : Total pore volume; V_{mic} : Micropore volume; V_{mes} : Mesopore volume calculated from subtracting total pore volume (at $P/P_0 = 0.99$) from micropore volume.

7.3.2 Thermal characteristics of catalyst and pyrolysis feedstocks

Before co-pyrolysis, the thermal stability of the synthesized Cu-Cr-ZSM-5 catalyst was evaluated by performing TG/DTG analysis by mixing the catalyst with a CLALG sample (Fig. 7.8). Different ratios of catalyst mixed with CLALG (0–100 %) were undergone thermal degradation at a heating rate of 10 ºC/min. Analysing TG results, increasing ratio of catalyst (0–100 %) with pyrolysis feedstock CLALG blends increases residual mass % from 40.21 % (CA-CLALG 0-1) to 93.83 % (CA-CLALG 1-0) as shown in Fig. 7.8. Correspondingly, maximum thermal decomposition rate reduces in the range of – 0.19 %/ ºC (CA-CLALG 0-1) to – 0.03 %/ ºC (CA-CLALG 1-0) as shown in Fig. 7.8.

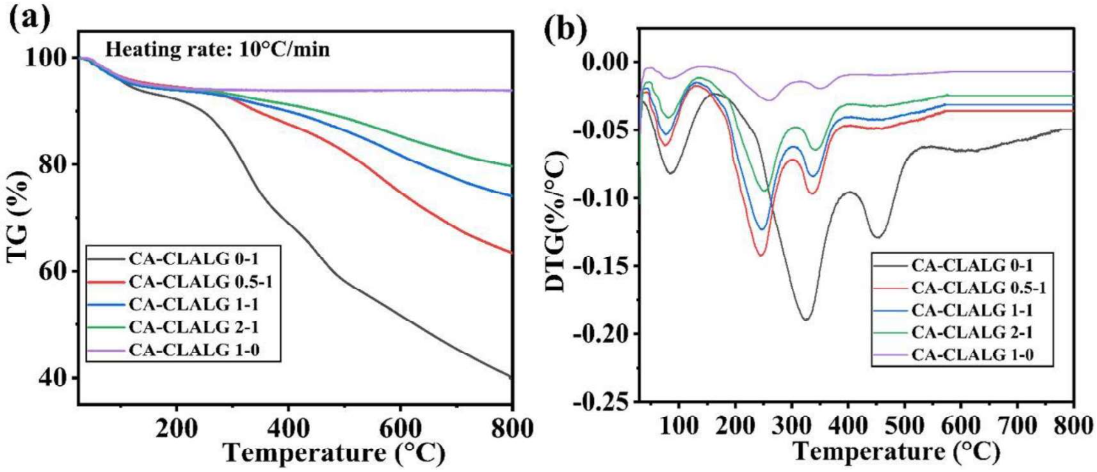

Fig. 7.8 (a) TG profile (b) DTG profile for coal and de-oiled microalgae blend with different ratios of catalyst. CA-CLALG 0-1, CA-CLALG 0.5-1, CA-CLALG 1-1, CA-CLALG 2-1, CA-CLALG 1-0; CA: synthesized Cu-Cr-ZSM-5 catalyst.

The maximum weight loss peak of synthesized catalyst is observed at 254 °C, consistent with reported study indicating maximum weight loss peak of ZSM-5 catalyst at 220 ºC (He et al., 2022). The two distinct weight loss regions are observed in DTG curve of the synthesized catalyst; first prominent peak corresponds to desorption of bounded water and other impurities from intramolecular region of supported matrix of catalyst (30–250 ºC, mass loss –5.77 %) and second peak corresponds to dihydroxylation (250–350 ºC, mass loss –0.61 %) which is comparable to reported literature (Khajevand et al., 2024). Further, thermal degradation of blends with catalyst ratio 0.5 to 2 lie between the TG profile of the catalyst and CLALG Fig. 7.8.

7.3.3 Product yield distribution from non-catalytic and catalytic pyrolysis

The product yield distribution (%) of bio-oil, char and gas from pyrolysis of CL, ALG and CLALG samples interacted with synthesized catalyst is shown in Fig. 7.9. To conduct ex-situ pyrolysis experiments, three different ratios of catalyst and feedstock (0.5:1, 1:1 and 2:1) were used to analyze the variation in char, bio-oil and gas production. The pyrolysis process was conducted at 600 °C (temperature), 60 min (residence time) and 10 °C/min (heating rate). Liquid obtained from non-catalytic/catalytic pyrolysis of feedstock typically consists of two different layers defined as the aqueous and organic phases (Pan et al., 2010). Both, organic phase (defined as bio-oil) and aqueous phase (enriched with water content) of liquid product were separated and weighed, respectively. After end product collection, yields (Y_{Char}, $Y_{Aqueous\ product}$, $Y_{Bio\text{-}oil}$ and Y_{Gas}) were calculated by using Eq. 7.1, Eq. 7.2 and Eq. 7.3, respectively (as explained in previous section 7.2.4), observed a higher bio-oil yield of non-catalytic pyrolysis over catalytic pyrolysis. The product yield distribution results indicate that non-catalytic CL pyrolysis produced a maximum of 15.5 % bio-oil, while it was gradually decreased for catalytic pyrolysis with an increasing catalyst ratio from 0.5 to 2 (Fig. 7.9). Conversely, more gaseous product was obtained for catalytic than non-catalytic pyrolysis with increasing catalyst ratio (0.5 to 2), in complete agreement with previous coal studies (Zhang et al., 2019). Increasing the catalyst mixing ratio with CLALG sample from 0.5 to 2, pyrolysis vapors interaction with catalyst takes longer time due to trapping of volatiles within the catalyst.

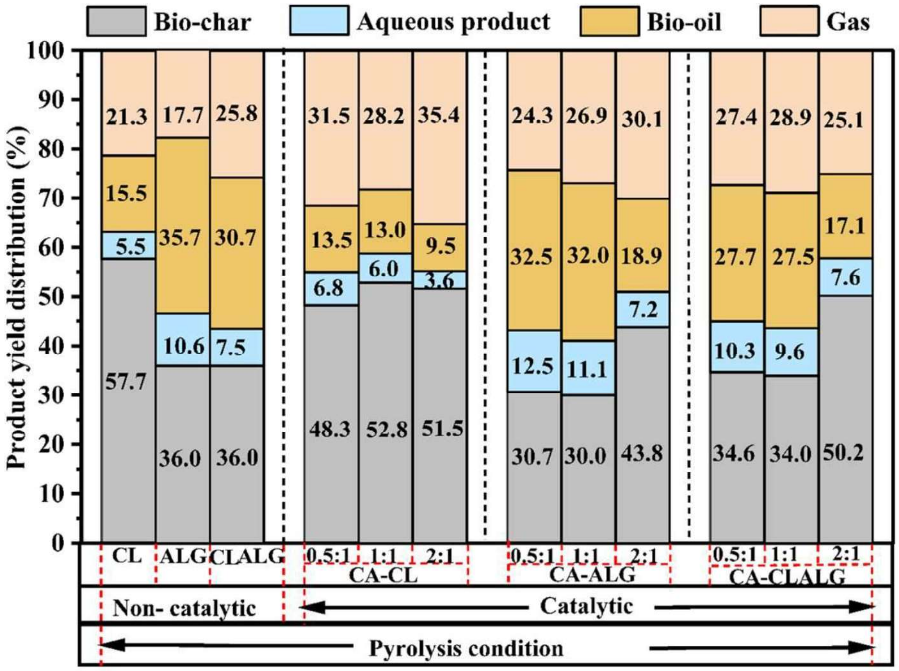

Fig. 7.9 Product yield distribution (%) of char, aqueous product, bio-oil and gas from non-catalytic and catalytic pyrolysis of coal (CL), microalgae (ALG) and coal-microalgae blend (CLALG) with the synthesized catalyst at different ratios (0.5:1, 1:1 and 2:1).

Further, it enhances the direct contact between heterogenous catalyst and feedstock, promoting thermal cracking and secondary reactions. The thermocatalytic cracking of these volatiles at active site of catalyst cause breaking of oxygenous and nitrogenous compounds through series of secondary reactions to lower bio-oil yield and production of CO_2, NO_x, SO_x or light hydrocarbons (Castello, 2019). External mass transfer limitation may be probable reason in slower diffuse out of volatiles across catalyst surface as catalyst ratio increases (Hoff et al., 2017). The shape and hierarchical pore structure of catalyst directly impacts the transport of molecules (Hoff et al., 2017). In this direction, novel catalyst formulations such as bifunctional catalysts, can improve pyrolysis oil yield (Cheng et al., 2011). Recently, catalytic fast pyrolysis at a high heating rate (10–200 ºC/s), moderate temperatures (400–600 ºC) and short residence time (< 5 s) are investigated to improvise quality and yield of bio-oil.

During catalytic pyrolysis, coal vapors were contacted with acid sites of synthesized catalysts. Excessive cracking activities include decarbonylation, dehydration, decarboxylation, and deamination reactions responsible for releasing functional groups and entrapment of volatiles inside the catalyst (Bi et al., 2020). This could cause a reduction in oil yield (%) during catalytic pyrolysis (Zhang et al., 2019). The distribution of products in non-catalytic pyrolysis indicates that ALG pyrolysis yields higher bio-oil (35.7 %) than coal (15.5 %), as shown in Fig. 7.9. The main reason was the excessive volatile matter content of ALG (43.01 %) than CL (13.5 %). In previous studies, it was reported that non-catalytic/direct pyrolysis of *S. obliquus*, *Chlorella vulgaris*, *Nannochloropsis sp.* and *S. platensis* produced bio-oil as 46.37 % (Mustapha et al., 2021), 52.7 % (Kumar et al., 2017), 58.1 % (Tang et al., 2021) and 43.6 % (Mo et al., 2020), respectively. Further, catalytic pyrolysis of ALG samples with 0.5:1 and 1:1 showed a slight reduction in bio-oil (32.5-32.0 %), which declined sharply for the 2:1 sample (18.9 %). It may be due to increasing the catalyst amount is not responsible only for the cracking of emitted pyrolysis vapors for oil upgradation but also for creating micropore diffusional resistance due to the trapping of vapors inside the catalyst surface (Bi et al., 2020). Among non-catalytic pyrolysis, CLALG yields 30.7 % bio-oil, close to the maximum bio-oil yield of 35.7 % (ALG), which shows synergistic interaction of CL and ALG during pyrolysis.

Considering no significant change in bio-oil yield distribution (%) for catalyst to feedstock ratio of 0.5:1 to 1:1 for all three combinations (CA-CL/CA-ALG/CA-CLALG), bio-oil characterization experiments (GC-MS/FTIR) were conducted for catalyst to feedstock ratio of 1:1 to analyze the impact of catalyst upon bio-oil quality.

7.3.4 Bio-oil characteristics from non-catalytic and catalytic pyrolysis

7.3.4.1 Fourier transform infrared spectroscopy of bio-oil

The FTIR analysis provides rapid quality estimation of bio-oil based on structural variation (Singh et al., 2020). In present study, FTIR spectra of non-catalytic and catalytic bio-oil (catalyst and feed ratio 1:1) of pyrolysis feedstocks CL, ALG and CLALG were performed to evaluate impact of catalyst interaction upon oil properties (Fig. 7.10).

FTIR spectra of non-catalytic CL bio-oil confirmed the excess presence of C–O stretching between 1058–1224 cm^{-1} correlated to primary alcohol which was reduced in catalytic coal bio-oil reflecting the deoxygenation reactions due to catalyst interaction as reported in literature (Bi et al., 2020). These results were comparable to bio-oil derived from different ranks of coal pyrolysis (Zhang et al., 2019). The catalytic pyrolysis oil samples, CL, ALG and CLALG show presence of O–H stretching at 1420–1330 cm^{-1} and 3700–3584 cm^{-1} corresponds to water and alcohol impurity in bio-oil samples, which is also reported by different catalytic pyrolysis studies as shown in Zainan et al. (2018). The presence of water impurity in catalytic bio-oil samples was correlated to the decarboxylation and deoxygenation action of the catalyst interacted with pyrolysis vapors Zainan et al. (2018).

In assertive agreement with FTIR analysis of bio-oil from *S. platensis* (Mo et al., 2020), non-catalytic ALG bio-oil showed the presence of high intense C=O stretching at 1706 cm^{-1}, which confirmed the availability of carboxylic acid. The spectra of both non-catalytic as well as catalytic ALG bio-oil showed sharp N–H and S=O stretching at 2919 cm^{-1} and 1380 cm^{-1}, corresponding to amine salt and sulfate respectively, due to significant protein content in de-oiled ALG (Fig. 7.10).

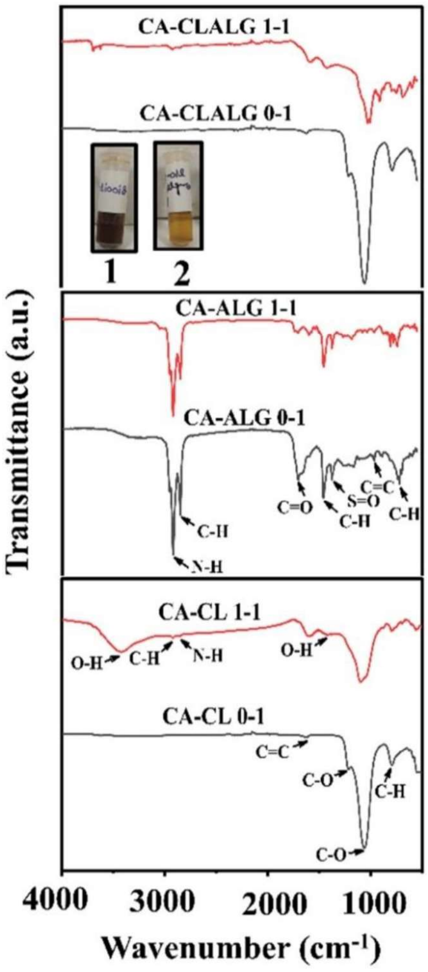

Fig. 7.10 FTIR spectra of bio-oil derived from non-catalytic and catalytic pyrolysis of coal (CL), microalgae (ALG) and coal-microalgae (CLALG) blend with synthesized Cu-Cr-ZSM-5 catalyst at ratio of 1:1. In Fig. 7.10, 1 and 2 represents visual appearance of non-catalytic and catalytic pyrolysis derived bio-oil.

Like coal bio-oil, catalytic bio-oil from CLALG showed no C–O stretching at 1216 cm^{-1}, confirming oxygen reduction in catalytic bio-oil (Bi et al., 2020). Similar to other reported studies, bands at 1619 cm^{-1}, 1593 cm^{-1} and 1627 cm^{-1} corresponded to C=C stretching in bio-oil from CL, ALG and CLALG pyrolysis at both catalytic and non-catalytic pyrolysis conditions (Mo et al., 2020).

7.3.4.2 GS-MS of catalytic and non-catalytic pyrolysis bio-oil

The quantitative estimation of catalytic and non-catalytic bio-oil of CL, ALG, and CLALG pyrolysis was performed through GC-MS analysis, and the GC-MS spectrum is presented in Fig. 7.11. The different carbon number compounds are presented in oil. Therefore, catalytic and non-catalytic bio-oil components of CL, ALG, and CLALG pyrolysis were classified based on carbon number (Fig. 7.11a. The catalyst interaction with pyrolysis volatiles significantly increased the < C10 compounds for all three feedstocks. It might be due to the thermocatalytic cracking of heavier to lighter hydrocarbons at the catalyst site (Dong et al., 2021).

In the present study, the catalytic effect was more significant for ALG, which showed a maximum increment of lighter hydrocarbons (71.3 %) than CL (27.5 %) and CLALG (60.7 %), as shown in Fig. 7.11a. The CL bio-oil is mainly composed of bulky heterocyclic aromatics and polyaromatic hydrocarbons constituting 68.5 % hydrocarbons of > C20 compounds. The bulky size of hydrocarbons in CL bio-oil hinders cracking and results in an inferior yield of light hydrocarbons (27.5 %) in accordance with previous coal pyrolysis study (Sardi et al., 2022).

During the pyrolysis process, heavier (> C20) compounds are mainly produced at a lower pyrolysis temperature, and secondary catalytic cracking of these heavier compounds cannot occur under low temperature conditions. However, lighter (< C10) compounds are mainly produced at higher temperatures (Dong et al., 2021). The porous structure of the synthesized Cu-Cr-ZSM-5 catalyst facilitates the adsorption of lighter compounds, and secondary cracking of lighter compounds occurs due to high thermocatalytic performance of the synthesized catalyst (Bi et al., 2020).

The catalytic cracking degrades C (10–20) compounds more efficiently. Hence, < C10 compounds can be easily separated from > C20 compounds by minimizing intermediate C (10-20) compounds (Dong et al., 2021). Further, carbon number distribution results for bio-oil derived from CLALG pyrolysis lie between CL and ALG (Fig. 7.11a). It was worth noting that catalytic action facilitated the easy separation of light hydrocarbons (< C10) from heavy hydrocarbons (> C20) by minimizing intermediate hydrocarbons from C10–C20 (Fig. 7.11a).

The oil characterization is also broadly classified based on the aliphatic hydrocarbon, aromatic hydrocarbon, N-compounds and O-compounds. In O-compounds, a higher relative content (%) of carboxylic acid in crude oil may cause corrosion and reduce oil’s heating value (Dhyani et al., 2018). So, the impact of catalytic thermocracking upon carboxylic acids is discussed independently from other oxygen compounds. According to GC-MS results, catalytic CL pyrolysis yields a higher content of aliphatic (40.37 %) and aromatic (8.69 %) hydrocarbons than ALG pyrolytic bio-oil with aliphatic hydrocarbon of 31.38 % and aromatic hydrocarbon of 5.34 % (Fig. 7.11b).

The catalytic interaction upgraded bio-oil quality with aromatic hydrocarbon selectivity of 54.4 %, 49.35 % and 50.11 % for CL, ALG and CLALG samples, respectively (Fig. 7.11b). The bio-oil from non-catalytic ALG pyrolysis contains significant nitrogen (22.1 %) and oxygen composition (24.1 %), due to thermolysis of protein and carbohydrate in de-oiled microalgae biomass as reported with other biomass pyrolysis (Mustapha et al., 2021).

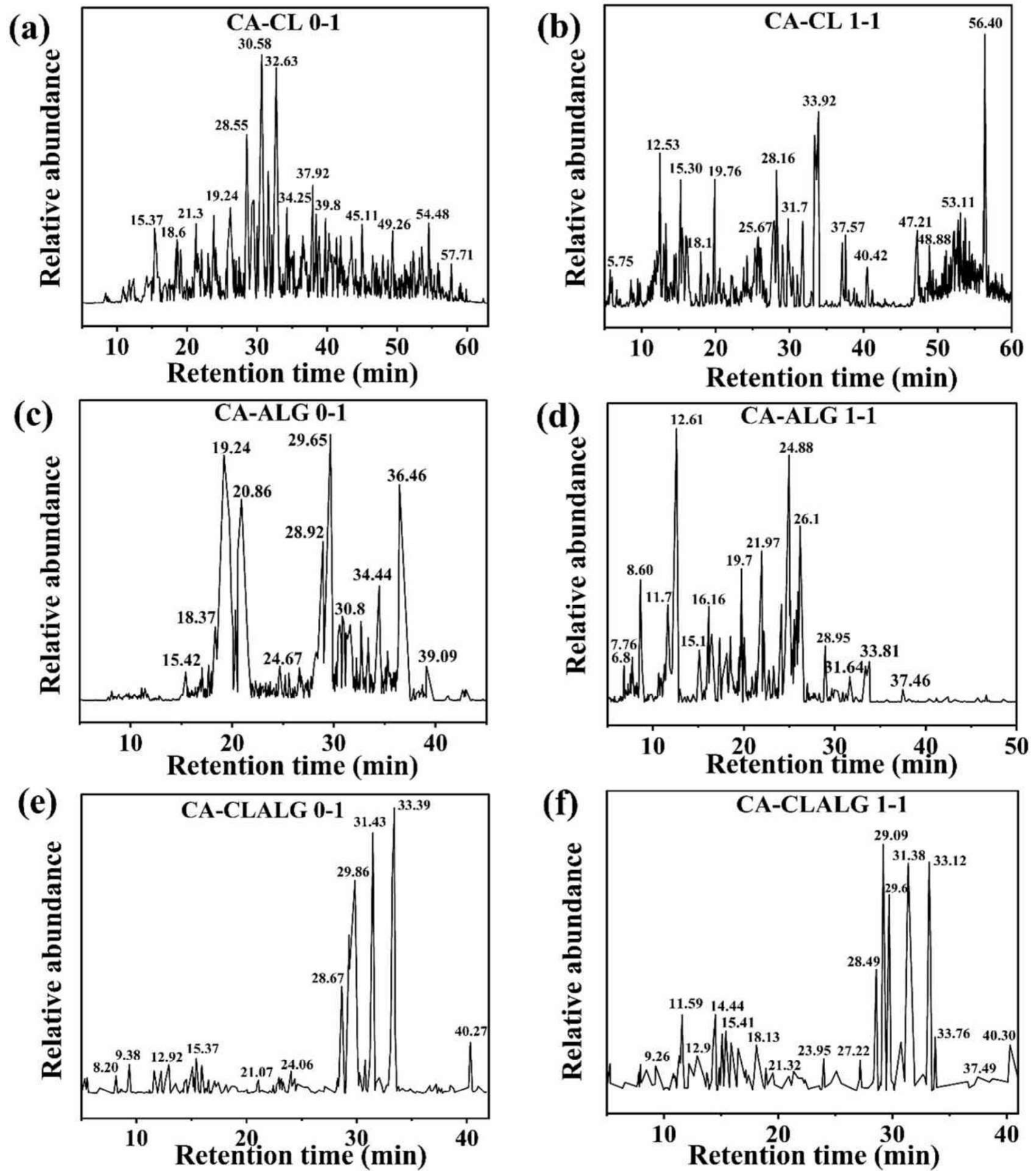

Fig. 7.11 GC-MS spectrum of bio-oil from pyrolysis of coal (CL), microalgae (ALG) and coal-microalgae (CLALG) blend (a, c, e) non-catalytic (b, d, f) catalytic respectively.

The catalytic denitrogenation and deoxygenation action reduced nitrogen content from 22.1 % (non-catalytic) to 5.1 % (catalytic) and oxygen content from 24.1 % (non-catalytic) to 2.2 % (catalytic) (Fig. 7.11b). The maximum carboxylic acid content of non-catalytic ALG pyrolysis bio-oil was reduced from 17.08 % to 10.2 % through catalytic conversion (Fig. 7.11b). The catalytic pyrolysis of *S. platensis* showed similar results with reduced N content of 1.25 % (Tang et al., 2021).

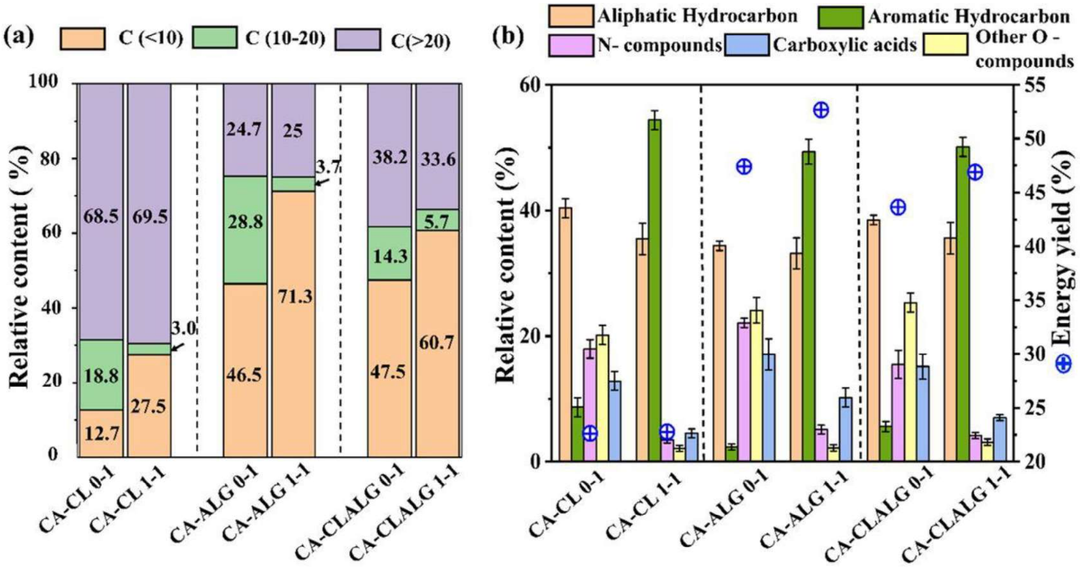

Fig. 7.12 Bio-oil component distribution from non-catalytic and catalytic pyrolysis (a) classification based on carbon number (b) chemical composition and energy yield of bio-oil.

In the present study, oxygen-containing components in bio-oil were grouped into five major categories – furans, phenols, acids, alcohols and ketones (Fig. 7.13). The presence of heteroatoms like bulky oxygenated compound such as acids are responsible for increasing oil viscosity, limit oil flow and reduce HHV (Li et al., 2020). Catalytic upgradation significantly reduced acid content to 4.5 %, 10.2 % and 7 % for CL, ALG and CLALG pyrolysis, respectively (Fig. 7.13). Excluding acids, other oxygen-containing components such as furans, phenols, alcohols and ketones are reduced to ≤ 1 % via catalytic pyrolysis of CL, ALG and CLALG (Fig. 7.13). The catalytic deoxygenation of pyrolytic bio-oil was similar to other studies that reported reducing acid content in bio-oil (nearly 4 %) by applying zeolite as a catalyst (Tang et al., 2021). Overall, catalytic interaction reduced oxygenated compounds remarkably, facilitating bio-oil enhancement for direct application in bio-refinery at a lower cost (Ukaew et al., 2018). Pyrolysis bio-oil is comprised of N heterocycles, amides, and nitriles as the main nitrogenous compounds. Bio-oil GC-MS analysis results showed that the synthesized catalyst could effectively reduce amides and nitriles (≤ 1 %) via catalytic pyrolysis of CL, ALG and CLALG (Fig. 7.14). The mesoporosity of the synthesized catalyst promotes the cyclization of amides/ amines to pyrrole and pyridine (Tang et al., 2021). Conversely, the synthesized catalyst did not strongly inhibit N heterocycles as amides/ nitriles. The catalyst interaction significantly dropped N yield from 22.1 % (non-catalytic) to 5.1 % (catalytic). Previous studies strongly recommend that more robust acid sites of zeolite-based catalysts promote nitrogen reduction from pyrolysis volatiles and facilitate more protons for hydrodenitrification (Wu et al., 2022).

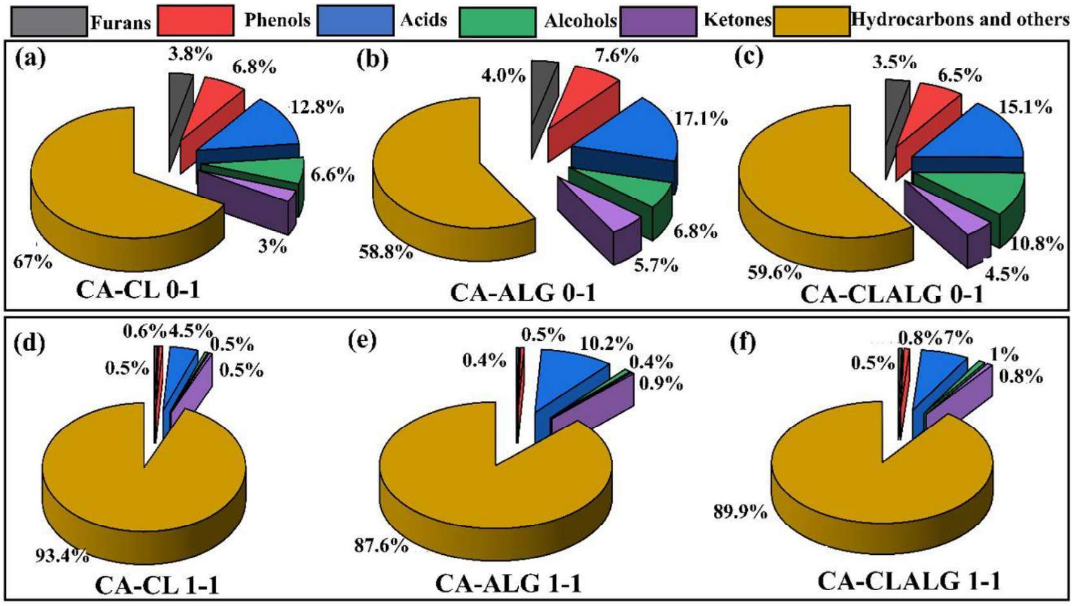

Fig. 7.13 The main oxygen components distribution in bio-oil from (a) non-catalytic (b) catalytic pyrolysis of coal (CL), microalgae (ALG) and coal-microalgae blend (CLALG) with synthesized Cu-Cr-ZSM-5 catalyst at a ratio of 1:1.

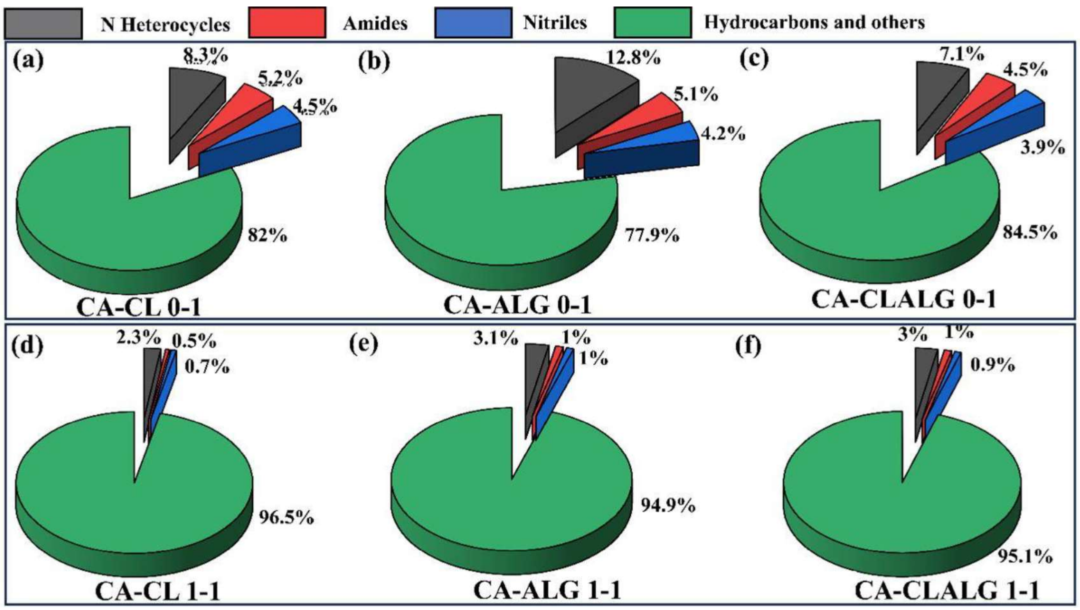

Fig. 7.14 The main nitrogen components distribution in bio-oil from (a) non-catalytic and (b) catalytic pyrolysis of coal (CL), microalgae (ALG) and coal-microalgae blend (CLALG) with synthesized Cu-Cr-ZSM-5 catalyst at a ratio of 1:1.

Overall, GC-MS analysis of CLALG pyrolysis (catalyst and feed ratio 1:1) showed a significant reduction in nitrogen and oxygen-containing components up to 4.16 % and 3.13 %, respectively, with enhanced aromatization up to 50.11 % aromatic content in bio-oil (Fig. 7.12b). The main chemical composition in bio-oil from catalytic and non-catalytic pyrolysis of CLALG is listed in Table 7.3.

Table 7.3 Main chemical components present in bio-oil derived from catalytic and non-catalytic pyrolysis of coal and de-oiled microalgae blends.

Chemical components	**Molecular formula**	**Relative content (Peak area %)**	
		Catalytic	**Non-catalytic**
Hydrocarbons			
2-Hexyne, 5-methyl-	C_7H_{12}	7.75	3.62
Cyclohexane, 1,2-bis(methylene)-	C_8H_{12}	4.93	2.87
Cyclopentane, 1,2,4-trimethyl	C_8H_{16}	2.87	1.22
1-Methylcyclooctene	C_9H_{16}	1.41	0.98
3-Nonyne	C_9H_{16}	1.97	0.71

Chemical components	**Molecular formula**	**Relative content (Peak area %)**	
		Catalytic	**Non-catalytic**
3-Heptene, 4-ethyl-	C_9H_{18}	1.18	0.87
1,4-Decadiyne	$C_{10}H_{14}$	1.52	1.87
Bicyclo [4.1.0] heptan-3-ol, 3,7,7-trimethyl-, [1S-(1. alpha.,3. alpha.,6. alpha.)]-	$C_{10}H_{16}$	2.72	1.04
1-Undecene	$C_{11}H_{22}$	1.06	0.8
1,5-Cyclooctadiene, 1-t-butyl	$C_{12}H_{20}$	0.39	0.81
3-Dodecene	$C_{12}H_{24}$	1.50	3.25
Cyclopentane, 2-n-octyl-	$C_{13}H_{24}$	0.82	0.50
Cyclohexane, 1,5-diisopropyl-2,3-dimethyl	$C_{14}H_{28}$	0.47	1.01
1,7-Dimethyl-4-(1-methylethyl) cyclodecane	$C_{15}H_{30}$	0.59	0.71
1, E-11, Z-13-Octadecatriene	$C_{18}H_{32}$	0.85	0.36
Cyclopropane,1-(1,2-dimethylpropyl)-1-methyl-2-nonyl-	$C_{18}H_{36}$	0.79	1.05
2-Hexadecene,3,7,11,15-tetramethyl-,[R-[R*,R*,E]]	$C_{20}H_{40}$	0.58	0.15
Cyclohexane, (1-octylnonyl)-	$C_{23}H_{46}$	2.75	1.5
Cyclohexane, (1-butylhexadecyl)-	$C_{26}H_{52}$	1.98	1.75
Octadecane, 3-ethyl-5-(2-ethylbutyl)-	$C_{26}H_{54}$	2.63	1.09
Cyclohexane, (2-decyldodecyl)-	$C_{28}H_{56}$	1.89	0.85
2-Methyloctacosane	$C_{29}H_{60}$	0.71	0.25
Tetratetracontane	$C_{44}H_{90}$	2.87	0.56
Oxygenated			
2-Furanone, 3,4-dihydroxytetrahydro	$C_4H_6O_4$	1.21	8.64
.beta-Methyl xyloside	$C_6H_{12}O_5$	1.68	7.84
Bicyclo [2.2.1] heptan-7-ol	$C_7H_{12}O$	0.52	5.98
5-trans-Methyl-1R,3-cis-cyclohexanediol	$C_7H_{14}O_2$	0.65	2.3
3-Octyn-1-ol	$C_8H_{14}O$	0.59	3.89
Benzenepropanoyl bromide	C_9H_9BrO	5.81	2.87
2-Hydroxy-3,5,5-trimethyl-cyclohex-2-enone	$C_9H_{14}O_2$	0.49	4.72
2,6-Nonadien-1-ol	$C_9H_{16}O$	0.78	4.2
2-Nonen-1-ol	$C_9H_{18}O$	0.71	4.54
Tetrahydrofuran, 2-hexyl-	$C_{10}H_{20}O$	0.37	4.10
2-Decen-1-ol, (E)-	$C_{10}H_{20}O$	0.27	3.67
2-(1,1-Dimethylethyl)-5-oxohexanal	$C_{10}H_{18}O_2$	1.87	8.5
.beta.-Phenoxyethyl acrylate	$C_{11}H_{12}O_3$	0.68	5.78
1,13-Tetradecadien-3-one	$C_{14}H_{24}O$	0.35	1.51
3-Tetradecyn-1-ol	$C_{14}H_{26}O$	0.49	4.01
Methyl 4,5-tetradecadienoate	$C_{15}H_{26}O_2$	0.39	7.85
Fumaric acid, dec-4-enyl octadecyl ester	$C_{32}H_{58}O_4$	0.15	8.89
Nitrogenous			
2-Aminopyridine	$C_5H_6N_2$	0.78	1.4
8-Azabicyclo [5.1.0] octane	$C_7H_{13}N$	0.6	1.1
endo-2-Aminonorbornane	$C_7H_{13}N$	0.52	1.78
5H-1-Pyrindine	C_8H_7N	0.49	1.2
3-Cyclohexen-1-nitrile, 6-methyl-	$C_8H_{11}N$	0.35	1.89
Piperazine, 1,4-diethyl-	$C_8H_{18}N_2$	0.23	1.5
Pyrimido[1,2-a]azepine, 2,3,4,6,7,8,9,10-octahydro-	$C_9H_{16}N_2$	0.19	1.89
2-Azatricyclo [4.3.1.1(4,8)] undecane	$C_{10}H_{17}N$	0.09	1.35
Cycloheptanone imine, 2,2,7,7-tetramethyl-	$C_{11}H_{21}N$	0.20	1.06

Chemical components	Molecular formula	Relative content (Peak area %)	
		Catalytic	Non-catalytic
Hexadecenenitrile	$C_{16}H_{29}N$	0.17	0.98
Acid			
(R)-(-)-4-Methylhexanoic acid	$C_7H_{14}O_2$	0.27	0.54
2-Octenoic acid, cis-	$C_8H_{14}O_2$	0.70	1.5
3-Tetradecanynoic acid	$C_{14}H_{24}O_2$	0.70	1.2
n-Hexadecanoic acid	$C_{16}H_{32}O_2$	0.31	2.0
Oleic acid	$C_{18}H_{34}O_2$	0.85	1.0
Oxygenated and nitrogenous compound			
Phenylethylene, 3'-methoxy-2,2'-dinitro-	$C_9H_8N_2O_5$	6.54	2.54
2,5-Piperazinedione, 3-methyl-6-(phenylmethyl)-	$C_{12}H_{14}N_2O_2$	3.89	0.87

7.3.4.3 Physicochemical characteristics of bio-oil from non-catalytic and catalytic pyrolysis

The physicochemical properties of non-catalytic and catalytic oil from CLALG pyrolysis were compared with mineral and ASTM-grade oils (Dhyani et al., 2018). Non-catalytic bio-oil had an intense dark brown color with no transparency, while catalytic bio-oil showed a dark yellow color with little transparency (Table 7.4). The pH of catalytic bio-oil was 32 % higher than that of non-catalytic bio-oil, which was rich in aliphatic acids and phenolic components (Table 7.4). However, catalytic interaction with volatiles during pyrolysis enhanced moisture content by 42 % as a limitation (Table 7.4).

Catalytic CLALG pyrolysis reduced ash % up to 0.02 with an increased HHV of 32.4 MJ/kg, comparable to reported mineral oil HHV of 40.6–42.6 MJ/kg (Dhyani et al., 2018). Further, bio-oil viscosity depends upon the nature of feedstock and processing conditions. Opposite to heavy fuel oil and ASTM grade oil, the viscosity of catalytic upgraded bio-oil was observed as 3.85 cSt, which lay in the range of light fuel oil (2.0–4.5 cSt), as shown in Table 7.4.

Focusing on the impact of metal-modified zeolite upon bio-oil quality, recent catalytic bio-oil pyrolysis of versatile feedstocks such as microalgae, lignocellulose and low-density polyethylene with waste cooking oil are compared with the present study

(Table 7.5). This analysis directly interprets that Cu and Cr-modified ZSM-5 upgrade oil more efficiently than single metal-modified or parent ZSM-5 in terms of deoxygenation, denitrogenation, and aromatization (Table 7.5). Furthermore, the highest obtained HHV of CL pyrolysis (40.1 MJ/kg) followed by CLALG (38.6 MJ/kg) and ALG (36.5 MJ/kg) pyrolysis is comparable to diesel oil with HHV (42–46 MJ/kg).

Table 7.4 Physicochemical comparison of bio-oil from catalytic and non-catalytic pyrolysis of coal and de-oiled microalgae blend with ASTM grade oil and mineral oils.

Properties	**Non-catalytic** [a]	**Catalytic** [a]	**Heavy fuel oil** [b]	**Light fuel oil** [b]	**ASTM-Grade D** [c]	**ASTM-Grade G** [c]
Appearance	Dark brown	Dark yellow	NA	NA	NA	NA
Water content, %	24.69	35	40.6	42.6	>15	> 15
Density (g/cm^3)	1.142	1.013	0.99	< 0.845	1.1–1.3	1.1–1.3
Viscosity (cSt) [d]	4.01	3.85	180–420	2.0–4.5	< 125	< 125
pH	2.28	3.01	NA	NA	NA	NA
Ash, %	0.04	0.02	< 0.08	< 0.01	< 0.15	< 0.25
Nitrogen, %	0.38	0.15	0.4	0.02	NA	NA
Sulphur, %	< 0.01	< 0.01	NA	NA	NA	NA
HHV (MJ/kg)	27.01	38.56	40.6	42.6	>15	>15

[a] Bio-oil from non-catalytic and catalytic pyrolysis of CA-CLALG 1-1(present study); [b] Heavy and light fuel oil (Chiosso et al.2023); [c] ASTM grade oil; [d] Viscosity measurement at 40 °C; NA: Not available.

Table 7.5 Summary of recently performed studies to upgrade pyrolysis bio-oil quality by applying different metal-loaded zeolite catalysts.

Pyrolysis feed stock	**Synthesized catalyst with loaded Metal (%)**	**Process condition (Rector type/ T_p / HR)**	**Catalytic bio-oil upgradation**				**Reference**
			O content % (w/w)	**N content % (w/w)**	**Aromatic content % (w/w)**	**HHV (MJ/kg)**	
Chlorella vulgaris	Ni-ZSM-5 (5 %)	Fixed bed reactor, 500°C, 10°C/min	< 15	23	15.2	NA	Yashnik et al., 2022
Spirulina platensis	MgO-ZSM-5 (10 %)	Fixed bed reactor, 800°C, 10°C/min	7.0	0.2	> 60	36.8	Mo et al., 2020
Scenedesmus obliquus	Co/Fe_3O_4-ZSM-5 (10 %)	Fixed bed reactor, 500°C, 10°C/min	9.38	4.77	10.5	39.1	Mustapha et al., 2021

Lignin	HZSM-5	Fixed bed reactor, 550°C, 10°C/min	5	NA	18	NA	Avila et al., 2024
Oak tree woodchips	HZSM-5	Continuous mode reactor, 500°C	10	0.5	8	36.7	Pagano et al., 2024
Low density polyethylene and Waste cooking oil	Ni-ZSM-5 (10 %)	Fixed bed reactor, 450°C	10	NA	47	NA	Qiu et al., 2023
(i) Low rank coal			2.1	3.5	54.4	40.1	Present study
(ii)De-oiled microalgae			2.2	5.1	49.4	36.5	Present study
(iii) Low rank coal and de-oiled microalgae blend			3.1	4.2	50.1	38.6	Present study

NA -Not available; T_p - pyrolysis temperature; *HR* - heating rate.

7.3.5 Proposed mechanism for catalytic upgradation of bio-oil applying synthesized Cu-Cr-ZSM-5 catalyst

In the present study, synthesized Cu-Cr-ZSM-5 catalyst exhibited efficient deoxygenation, denitrogenation and aromatization action in catalytic upgradation of CL, ALG and CLALG pyrolysis volatiles to yield high quality bio-oil. The catalytic upgradation mechanism of bio-oil derived from CLALG pyrolysis was proposed based on ex-situ induction of synthesized Cu-Cr-ZSM-5 catalyst (Fig. 7.15).

A typical coal structure is mainly composed of oxy-aromatic, alkylated aromatic and protonated aromatics (Chen et al., 2021). However, carboxylic acids, long-chain fatty acids, phenols and bulky oxygenated compounds are the main components of carbohydrate and protein rich de-oiled microalgae biomass (Kocer and Ozçimen, 2022). At the initial pyrolysis stage, the thermal decomposition of CL and ALG produced H_2O vapors. The dehydrogenation of oxygen-containing groups such as –COOH and –OH is responsible for internal moisture removal (Chen et al., 2021). The long aliphatic chains in pyrolysis feedstock is converted into light olefins during thermal cracking (Fig. 7.15).

The thermal decomposition of oxygen-containing functional groups such as –COOH, R–COO–R' and CH_3O released CO and CO_2 via decarboxylation reactions (Hu et al., 2024). In ALG biomass, nitrogenous compounds consisting mainly of amine group ($–NH_2$) as the basic unit in protein are responsible for removing ammonia during thermal cracking (Su et al., 2023). Further, acyl or alkoxy bond cleavage releases CO during thermal decomposition of long-chain fatty acids (Mishra et al., 2022). A significant fraction of NO_x is released from microalgae by the thermal decomposition of nitroalkyl and nitrophenyl compounds (Mo et al., 2020). Moreover, a small fraction of SO_x is also emitted by bond cleavage from dimethyl sulfoxide and methyl sulfide (Tang et al., 2021).

The emitted primary pyrolysis vapors from thermal decomposition of CL, ALG and CLALG were dominated with aliphatic hydrocarbons, bulky oxygenated compounds, carboxylic acids and nitrogen-containing compounds responsible for undesired properties in resulting non-catalytic bio-oil with low HHV. To upgrade non-catalytic bio-oil, the synthesized Cu-Cr-ZSM-5 catalyst is interacted with CLALG pyrolysis vapors. The controlled Si/Al ratio, pore size, mesoporosity, unique channels with circular entrances and acid sites are the specific parameters to impact deoxygenation and aromaticity of upgraded bio-oil (Zhang et al., 2018). Intramolecular mesopores of synthesized catalyst facilitate molecular diffusion and promotes pyrolysis vapours transformation at specific acidic site. The abundant mesopores and larger external surface area are responsible for accessible acid sites to interact with pyrolysis vapors (Iliopoulou et al., 2012). Excess inter/intra crystal mesoporosity overcome mass transfer limitations to improvise bio-oil quality with higher mono aromatic hydrocarbon yield (Zhang et al., 2018).

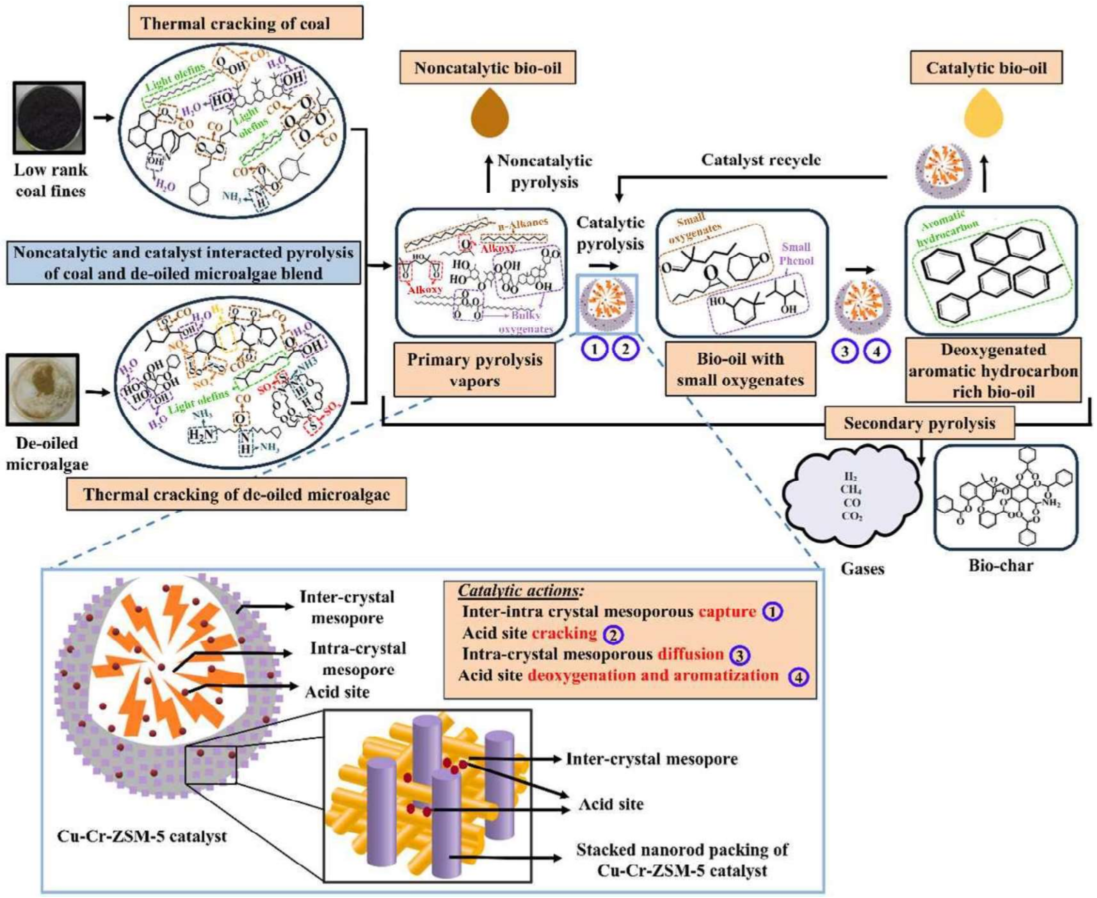

Fig. 7.15 Proposed reaction pathway of noncatalytic and catalytic pyrolysis of coal and de-oiled microalgae blend (CLALG) with synthesized Cu-Cr-ZSM-5 catalyst.

Further, mesoporous shells hinder the production of polyaromatic hydrocarbon. The acid sites in synthesized catalyst facilitate deoxygenation and other decoomposition reactions (Iliopoulou et al., 2012). Mesoporous synthesized Cu-Cr-ZSM-5 catalyst allow entry and access of larger macro-oxygenates into the inner zeolite acid sites. Enhanced mesoporosity and corresponding increase in accessible acid sites result higher conversion of medium and large oxygenates to the smaller oxygenates with improved bio-oil quality (Palizdar et al., 2020). A series of catalytic actions are supposed to occur at external catalytic acid sites, such as (i) side chain dealkylation to reduce the carbon number in hydrocarbon, (ii) coupled dehydrogenation-aromatization to produce naphthalene and another aromatic hydrocarbon with H_2 as a side product, (iii) hydrocracking to reduce heavy hydrocarbons to light hydrocarbons, (iv) coupled dehydration- hydrocracking to reduce oxygenated pool such as phenol content, (v) hydro denitrogenation by reduction of N-heterocycles to pyrrolic-N, pyridinic-N, amine/amide-N, as reported in previous studies (Bi et al., 2020).

In continuation, it is expected that catalytic acid sides supported the pre-cracking of bulky oxygenates from CLALG such as paromomycin, vanillin, tetra acetyl-d-xylonic nitrile, levoglucosenone to small oxygenates and alkyl/alkoxy phenols such as oxirane, furan, cis-2,3-epoxyoctane and 8-oxabicyclo octane. After intercrystal capturing of primary volatiles, intracrystal mesopores facilitate the cracking of active oxygenates and rapid diffusion of small oxygenates (Fig. 7.15). An array of deoxygenation and denitrogenation reactions occurred at inner acid sites to reduce oxygen and nitrogen containing components from bio-oil derived from CLALG pyrolysis. Additionally, catalytic pyrolysis induces mononcyclic aromatic hydrocarbon production at catalytic acid site. In this direction, a strong correlation between zeolite properties and selectivity of aromatic hydrocarbons was reported in a previous study (Wu et al., 2022). The mesoporosity, shape specificity and moderate acidity of synthesized ZSM-5 catalyst are key factors for the aromatization of pyrolysis vapors (Kim et al., 2019). These possible reaction mechanisms generate value-added products such as higher yield of light aromatics (< C10 carbon) with reduced oxygen and nitrogen-containing compounds. In view of catalyst morphology, aligned nanorods aggregated crystal structure with well-distributed mesopores also play crucial role to enhance bio-oil quality (Wu et al., 2022). After completing catalytic processing, value-added end products of pyrolysis vapors are rapidly diffuse out from the intra/inter crystal mesopores of the catalyst. The possible catalytic reactions and rearrangements proposed in present CLALG pyrolysis are in agreement with the reported catalytic mechanism of coal pyrolysis (Sardi et al., 2022) as well as microalgae pyrolysis (Tang et al., 2021). The secondary pyrolysis is further dominated at higher temperatures (> 600 °C) and carbonization of higher volatile matter generates char and gases in both non-catalytic and catalytic pyrolysis (Fig. 7.15).

7.4 Conclusion

The present study demonstrated catalytic upgradation of co-pyrolysis volatiles from low rank coal and de-oiled microalgae blends to allow maximum energy recovery in the form of carbon-neutral liquid fuel as bio-oil. Bimetallic (Cu and Cr) substituted mesoporous ZSM-5 is used for catalytic upgradation of bio-oil. Enhanced mesoporosity, moderate acidity and specific active sites of synthesized Cu-Cr-ZSM-5 catalyst act synergistically to enhance bio-oil quality with improved selectivity of aromatic hydrocarbon (49.4–54.4 %) and light (< C10) hydrocarbon (27.5–71.3 %). On comparing noncatalytic and catalytic bio-oil properties, it is worth noting that a significant drop in oxygen compounds (25.13 to 3.13 %) and nitrogen compounds (15.49 to 4.16 %) is observed in bio-oil from coal and de-oiled microalgae pyrolysis. These results indicate that catalytic conversion of bio-oil will able to provide oil combustion with reduced $CO/CO_2/NO_x$ emission. The significant 42.76 % increment in HHV is observed by catalytic upgradation of bio-oil from coal and de-oiled microalgae pyrolysis. HHV of coal pyrolysis bio-oil (40.1 MJ/kg) is very close to diesel oil (42–46 MJ/kg), which encourages coal liquefaction technologies towards transport fuel oil production. The current study suggests that future work must be implemented in the direction of oil yield improvement, low-cost catalyst preparation and application of advanced pyrolysis technologies with detailed techno-economic evaluations to ensure the feasibility of bio-oil as a transportation fuel.